Engineering Structures 77 (2014) 193–206

Contents lists available at ScienceDirect

Engineering Structures

journal homepage: www.elsevier.com/locate/engstruct

Real-scale CFD simulations of fire in single- and double-track railway tunnels of arched and rectangular shape under different ventilation conditions

Aram Amouzandeh [a,*], Matthias Zeiml [a,b], Roman Lackner [c]

[a] Institute for Mechanics of Materials and Structures, Vienna University of Technology, Karlsplatz 13, 1040 Vienna, Austria
[b] FCP – Fritsch, Chiari & Partner ZT GmbH, Diesterweggasse 3, 1140 Vienna, Austria
[c] Material-Technology Innsbruck, University of Innsbruck, Technikerstraße 13, 6020 Innsbruck, Austria

ARTICLE INFO

Article history:
Available online 7 June 2014

Keywords:
Tunnel fire
Tunnel lining
Ventilation
Heat transfer
Radiation
OpenFOAM

ABSTRACT

The development of measures to avoid or minimise the destructive effects of fires in tunnels requires a quantitative assessment of the thermal intake of the structure during such incidents. In the underlying work, a typical tunnel-fire scenario is analysed with the help of *Computational Fluid Dynamics* (*CFD*) in order to predict temperature distributions inside the tunnel which in turn shall be used to assess the structural stability of the concrete lining. The CFD simulations are based on a fire code previously developed within the framework of OpenFOAM. The fire is simulated in an arched single-track, an arched double-track and a rectangular double-track cross-section of real dimensions taking into account two different ventilation velocities (0.5 and 3 m/s). Results are compared in terms of temperature distributions within the cross-section and longitudinal temperature distributions at ceiling level. Except for the temperature distribution within the cross-sections, little difference in results is seen for the two double-track tunnels with the low ventilation velocity (0.5 m/s), whereas higher temperature levels and a faster downstream movement of hot gases are observed in the single-track tunnel. For the high ventilation velocity (3 m/s), temperature levels drop dramatically and flow parameters within the three tunnel cross-sections differ insignificantly. In addition, a comparison of temperature profiles inside the concrete tunnel lining with results of a more detailed 1D calculation is presented. In order to obtain the most accurate temperature profiles, a procedure is suggested, where the 1D heat-conduction equation is solved by using the fluid temperatures from a previous CFD simulation, taking into account the temperature dependency of thermo-physical parameters of concrete and, if necessary, the risk of spalling.

1. Introduction

In recent years, fire accidents in underground infrastructures caused numerous casualties as well as an immense economic loss as summarised, e.g. in [1]. In tunnel fires, the temperature loading causes significant thermal degradation of concrete. Additionally, spalling of near-surface concrete layers is likely to take place, further putting the integrity of the load-carrying structure at risk. In order to better understand the effects of the released heat on the tunnel structure, numerous tunnel-fire experiments were conducted. The results of the experiments like *Heat Release Rate* (*HRR*)-time and temperature-time curves, smoke production and smoke movement were presented and summarised in various publications (e.g., [1–6]). However, tunnel-fire experiments involve high costs and efforts, thus, making it difficult to conduct parametric studies. Thanks to increasing computational performance, simulations of fire scenarios by means of *Computational Fluid Dynamics* (*CFD*) represent a promising tool nowadays. It is a valuable method for sensitivity analysis with respect to different parameters, reducing experimental effort. The fact that CFD makes all physical variables at all points in space and time of the resolved scales accessible, it complements experimental investigations, and therefore, represents a powerful tool for efficient research in the field of fires in enclosures.

The approach followed for fire simulations applying CFD is depicted in Fig. 1: based on the evolution of the fire's heat-release rate, the CFD analysis allows to assess the evolution of the surface temperature of the structure at risk. The obtained information on absorbed thermal energy by the structure serves as boundary condition for a more detailed computation of the temperature

* Corresponding author. Tel.: +43 1 681 10 87 17 63.
E-mail addresses: aram.amouzandeh@gmail.com (A. Amouzandeh), matthias.zeiml@tuwien.ac.at, zeiml@fcp.at (M. Zeiml), roman.lackner@uibk.ac.at (R. Lackner).

http://dx.doi.org/10.1016/j.engstruct.2014.05.027
0141-0296/

Nomenclature

A	cross-sectional area (m^2)
c_p	specific heat capacity (J/kg/K)
d	distance (m)
D^*	characteristic plume diameter (m)
Δh_C	heat of combustion (J/kg)
$\dot{m}$	mass flux (kg/s)
q_w	specific wall-heat flux (W/m^2)
Q_w	absolute wall-heat flux (W)
$\dot{Q}$	burning or heat-release rate (W)
t	time (s, min)
T	temperature (K, °C)
U	velocity (m/s)
x, y, z	coordinates (m)
y^+	dimensionless wall distance (1)

Greek symbols

α_c	conv. heat-transfer coefficient ($W/m^2/K$)
α_q	quadratic growth coefficient (W/s^2)
α_d	exponential decay coefficient (s^{-1})
ε	surface emissivity (1)
λ	thermal conductivity (W/m/K)
ρ	density (kg/m^3)
σ_{SB}	Stefan–Boltzmann constant ($W/m^2/K^4$)

Subscripts

0	start, initial conditions
∞	ambient conditions
d	double-track
f	fluid
max	maximum
s	single-track
tot	total
ub	unblocked
w	wall

development inside the solid. In case of concrete, temperature distributions can be calculated by considering the coupling of thermo-hydro-chemical transport processes in order to assess the risk of spalling and, thus, the structural safety [7,8].

In the past, many researchers used the benefits of CFD to conduct parametric studies of tunnel fires. In [9], fires in an arbitrary 300 m long tunnel were simulated using CFD in order to investigate the influence of different parameters such as tunnel width and ventilation velocity on the spreading rate of hazardous hot gases and smoke. The results show the expected reduction of the spreading rate of hazardous hot gases with increasing ventilation velocity and that a smaller tunnel width leads to a faster propagation of smoke and hot gases in case of small fires (<30 MW). In [10], fire tests in a model tunnel and corresponding CFD simulations were carried out to investigate the influence of tunnel geometry and HRR on the critical velocity to prevent back-layering. A simple formula in dimensionless form for the critical velocity was developed. In [11], CFD was applied to study the influence of the tunnel's aspect ratio, i.e. tunnel height to tunnel width, on the smoke movement. Decreasing fluid temperatures close to the ceiling as well as a slower longitudinal temperature decay due to reduced heat loss to the smaller ceiling surface with increasing aspect ratio were observed by the authors. Similar studies were carried out by Ref. [12] revealing the strong effect of tunnel width on the shape of the fire plume due to a noticeable restriction of air entrainment in case of a narrow tunnel. The length of back-layering, the flame length and the effects of a blockage in large-scale tunnel fires were analysed with CFD in [13]. It is shown that the presence of an object in the tunnel, the HRR and the ventilation velocity strongly influence the flame length. In addition, a reduction of the critical velocity due to an object in the tunnel is observed. In [14], fire experiments in a scaled model tunnel with an arched cross section were re-analysed by means of CFD. The numerical simulations allowed to identify the impact of different ventilation regimes on the heat transfer to the walls, where less energy is transferred in the over-critical regime.

The underlying paper describes a case study of tunnel fires, where besides the fluid temperature, heat transfer to and the temperature development inside the tunnel lining is investigated. Results of CFD simulations of a fire in real-scale railway tunnels with three different cross-sections, i.e. (i) an arched single-track, (ii) an arched double-track and (iii) a rectangular double-track cross-section, are presented. Considering a high and low ventilation velocity (0.5 and 3 m/s), the CFD analysis should allow to estimate temperature distributions within the cross-sections and the evolution of longitudinal temperature distributions at ceiling level in order to provide realistic temperature data to assess the structural safety of the tunnel lining. Hereby, the main focus lies on the identification of the 450 °C gas layer at ceiling level, the fluid temperature which according to the Swiss standard SIA 197/1 [15] and preliminary versions of the *Technical Specification of Interoperability on Safety in Railway Tunnels* (*TSI SRT*) [16] shall be used to "*demonstrate that the integrity of the tunnel lining is maintained [...].*" Thus, the prediction of smoke production and smoke compo-

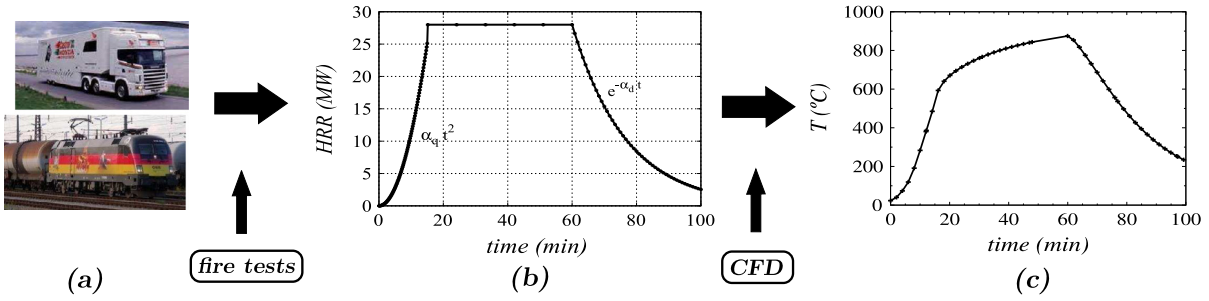

Fig. 1. Application of CFD for the simulation of fires in enclosures: (a) type of fire load, (b) evolution of HRR, and (c) evolution of surface temperature at a specific point within the tunnel.

sition is not of main interest in the underlying study. All presented results are produced with a fire code which was previously developed within the framework of OpenFOAM [17].

2. Applied CFD-code

The applied fire code was developed based on the open source CFD software OpenFOAM, Version 1.7.1 [18]. The solver couples conjugated heat transfer in a solid to a buoyancy-driven flow of a compressible Newtonian fluid at low Mach number. For turbulence modelling, a buoyancy-modified standard k–ε turbulence model based on the *Simple Gradient Diffusion Hypothesis* (*SGDH*) [19,20] is applied. In addition to the convective heat transfer within the fluid region, transfer of thermal radiation is considered with the *Finite Volume Discrete Ordinate Method* (*fvDOM*) [21] in a participating and grey medium, where scattering by gas molecules can be neglected according to [22]. Since soot production is not modelled here, the fluid is regarded as non-scattering. A simple combustion model based on the approach of a conserved scalar, i.e. the mixture-fraction [19,23], and with the assumption of mixing-controlled conditions is used to simulate the combustion process. Hereby, the mean consumption rate of fuel is calculated using the *Eddy Dissipation Model* (*EDM*) [24]. The fire is modelled as a buoyant turbulent diffusion flame which is fed by a prescribed mass flow of fuel corresponding to a HRR-time curve of the fire (see Fig. 1(b)). In [17], a detailed description of the code's development and its application to real-scale fire experiments is presented. In the following, a short description of the re-analysis of a tunnel-fire test with the mentioned code shall be given.

2.1. Re-analysis of tunnel-fire test

For the re-analysis, Test 2 of the 9 tunnel-fire tests in the 366 m long *Buxton Dust Explosion Gallery* [2] was considered. The test involved a kerosene pool fire as heat source in a 1:3-scaled model of a train used to carry heavy-goods vehicles (HGV). The geometry of the tunnel's cross-section with an area of 5.6 m^2 is depicted in Fig. 2 (*left*). Throughout the test, the gallery was ventilated with a constant average velocity of 1.1 m/s. *Oxygen Consumption Calorimetry* was used to estimate the HRR-time curve of the heat source shown in Fig. 2 (*right*) with a maximum HRR of 2 MW, representing the main input parameter for the CFD simulation.

The simulation results of the tunnel fire exhibit a realistic flow field and temperature distribution where the experimentally observed back-layering of hot gases against the ventilation direction can be identified (see Fig. 3). However, the results show an overestimation of the fluid temperatures near the fire with respect to the measurements (see Fig. 4 (*left*)). A similar behaviour was observed directly above the fire source during the analysis of the combustion model presented in [17]. Nevertheless, the overestimation of the temperatures in the present investigation is mainly attributed to the assumption of mixing-controlled conditions used in the combustion model. While the assumption is realistic in well-ventilated regions, such a region cannot be expected to exist at the position of the fire source in the HGV-carrier (x = 0 m). On the other hand, the predicted temperature evolution at 44.5 and 111.5 m downstream of the fire exhibit reasonable agreement with the evolution seen in the experiment (see Fig. 4 (*middle*) and (*right*)). Hence, the predictions of the developed fire code overestimate fluid temperatures in the vicinity of the fire source but show good correspondence with experimental data further downstream of the fire. Though further simulations of test cases need to be conducted for a systematic validation of the fire code, the outcome of the re-analysis of fire experiments (see [17] for a detailed description) suggests the application of the code to study other tunnel-fire scenarios.

3. Real-scale simulations

Three types of double-track railway-tunnel cross-sections are investigated, i.e. an arched single-track, an arched double-track and a rectangular double-track cross-section (see Fig. 5 with the cross-sectional areas listed in Table 1). The blockage's geometry complies with the railway-loading gauge GC, defined by the *International Union of Railways* (*UIC*) [25] representing a double-decker coach as used, e.g. by the Austrian Federal Railways (*Österreichische Bundesbahnen* (*ÖBB*)). The fire source (located at x = 0 m) is placed 5 m upstream of the upstream end of the blockage at a height of 2 m (see Fig. 6). The evolution of the fire's HRR is derived from the HRR-time curve of a passenger carrier with a peak value of 25 MW, given by the *Deutsche Bahn* [26]. In the underlying case, a periodic fire spread to waggons at downstream positions is assumed, temporarily leading to a maximum HRR of 34 MW which after averaging gives a constant peak value of 28 MW (see Fig. 1(b)). Furthermore, a faster fire growth than suggested in [26] is prescribed, taking into account the excess oxygen in case of fire in a moving train. Hence, a fully developed fire is attained at 15 min corresponding to a growth rate of α_q = 31 W/s^2. Starting at 60 min, an exponential decay with a coefficient of α_d = 0.001 s^{-1} [27] is assumed, with the total duration of the fire being then equivalent to the combustion of two waggons. The same assumptions (except for fire duration and decay) were used to develop a design-fire scenario for ventilation design in the *Semmering-Basistunnel Neu, Austria* [28].

The fires in the different types of cross-section are studied assuming two ventilation velocities (0.5 and 3 m/s, respectively) which cover two limits of typical ventilation velocities in tunnels. In order to avoid possible instabilities during the CFD simulations when applying a zero ventilation velocity, the value of 0.5 m/s was chosen to define an initial velocity field inside the tunnel. Hence, the lower limit of 0.5 m/s might be considered as the case of a very low natural ventilation velocity which can be caused by

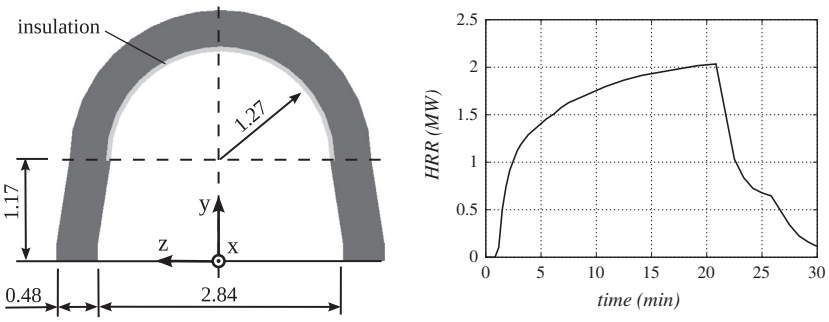

Fig. 2. Geometry of tunnel cross-section (*left*, dimensions in m), and HRR-curve (*right*) of the Buxton tunnel-fire Test 2 [2].

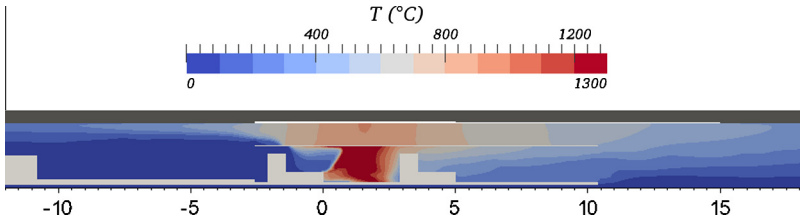

Fig. 3. Contour plots of temperature at $z = 0$ m for $t = 15$ min (dimensions in m, the position of the fire source corresponds to $x = 0$ m).

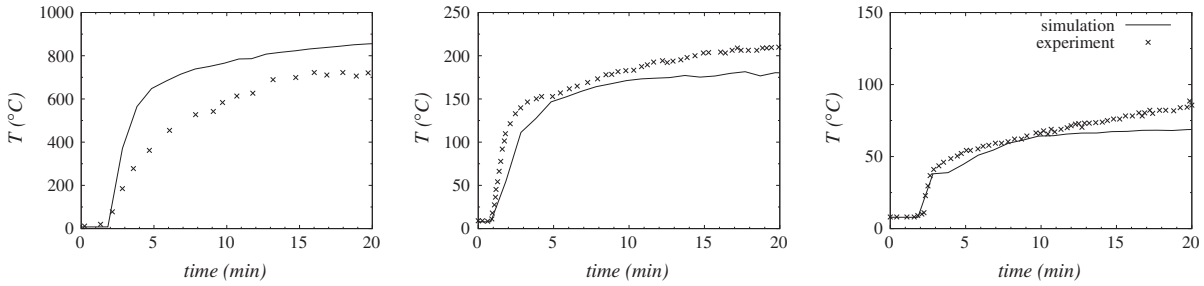

Fig. 4. Temperature evolution at the symmetry axis of the tunnel cross-section ($z = 0$ m) above the fire (*left*, $y = 2.17$ m), 44.5 m downstream of the fire (*middle*, $y = 2.21$ m) and 111.5 m downstream of the fire (*right*, $y = 1.75$ m).

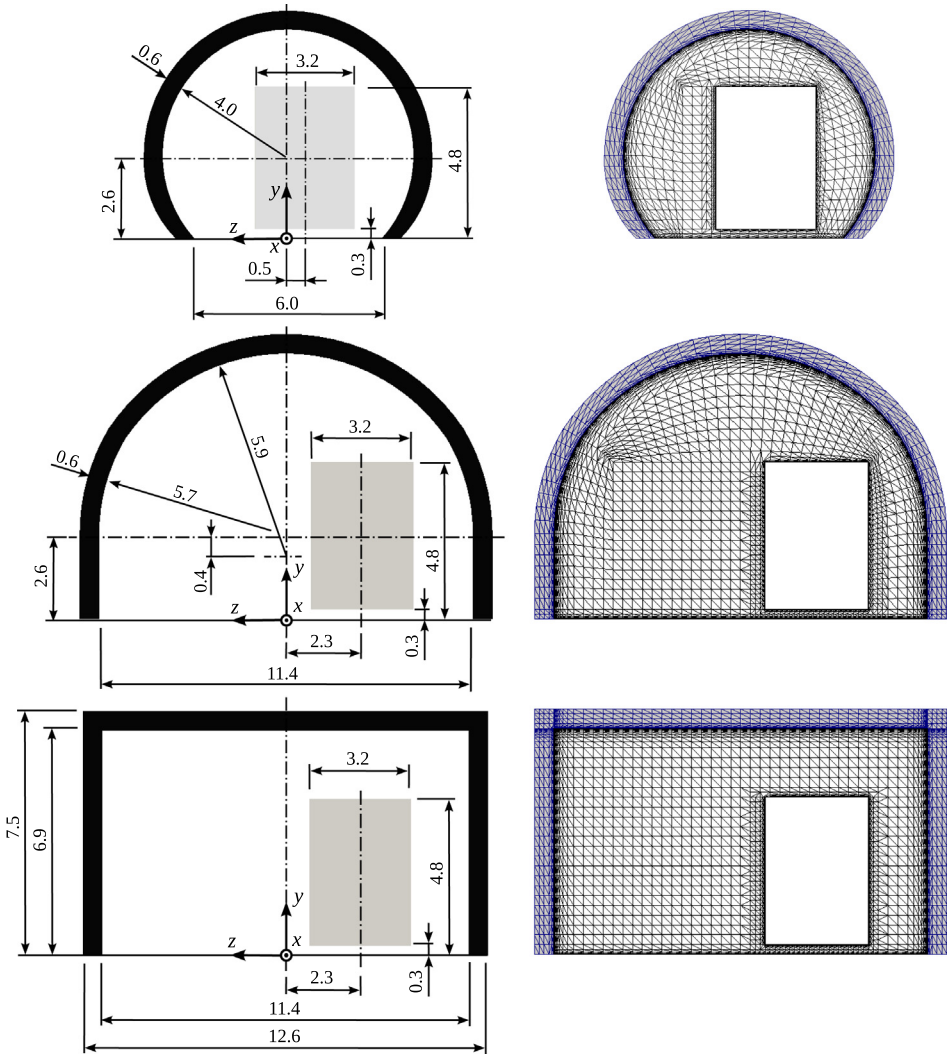

Fig. 5. Geometry (*left*, dimensions in m), and solid and fluid grids (mesh is triangulated by a post-processing artifact) at a cross-section far downstream of the fire (*right*) for the arched single-track (*top*), arched double-track (*middle*) and rectangular double-track (*bottom*) cross-section.

Table 1
Cross-sectional areas and area ratios of the single- and double-track tunnel cross-sections.

Tunnel type	Inflow area A (m^2)	Unblocked area at position of train, A_{ub} (m^2)	$\frac{A_{ub}}{A}$	$\frac{A_s}{A_d}$	$\frac{A_{ub,s}}{A_{ub,d}}$
Single-track *(s)*	44	30	0.68	0.56	0.46
Double-track *(d)*	79	65	0.82		

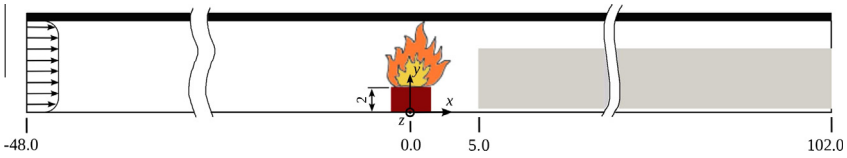

Fig. 6. Longitudinal cut through the middle of the train indicating the tunnel ventilation at the tunnel inlet (dimensions in m, $x = 0$ m corresponds to the location of the fire source).

the pressure difference between inlet and outlet of the tunnel due to meteorological effects. On the other hand, the ventilation velocity of 3 m/s represents a limit of the critical velocity needed to avoid back-layering for typical fire scenarios. In [6], different correlations for the critical velocity are studied and different experiments are presented aiming at identifying the critical velocity as a function of the HRR, also suggesting 3 m/s as upper limit for the critical velocity.

For all the presented CFD simulations, the following numerical set-up was employed:

- ***Grid:*** the computational grid extends from 48 m upstream to 102 m downstream of the fire source (see Fig. 6). The grid size of the hexahedral base meshes (see Fig. 5 (*right*)) of 0.3 m is estimated from a characteristic plume diameter of $D^* \approx 3.7$ m by using $D^*/10$ [29]. The grids are refined at the burner outlet, around the blockage and in areas adjacent to the tunnel lining to keep the dimensionless wall distance to $30 < y^+ < 100$ for a correct application of the wall-function approach [30], and are coarsened towards the outlet.
- ***Boundary conditions:*** at the tunnel inlet, a developed velocity profile corresponding to the desired ventilation condition of 0.5 and 3 m/s, respectively, is prescribed. The fluid enters the tunnel with an ambient temperature of 291 K (18 °C). The floor and the train are considered as adiabatic, whereas conjugate heat transfer including radiation and the application of temperature wall-functions are applied at the fluid-tunnel lining interface. The surface emissivity, ϵ, of all surfaces is set to 0.8 [31]. For the boundary condition at the concrete tunnel lining, the conjugate heat transfer is enabled at the fluid interface, whereas a constant temperature of 291 K (18 °C) is assumed at the remaining boundary interfaces (e.g. rocks).
- ***Initial conditions:*** the initial velocity field is obtained from an incompressible, isothermal simulation with the developed velocity profile at the inlet and including the blockage. The initial temperature field is set to 291 K (18 °C) in all regions.
- ***Heat source:*** the fire is modelled by a methane burner with a quadratic fuel inlet of 3 m side length at the position depicted in Fig. 6. At the fuel inlet, a time-dependent fuel mass-flow rate is specified which is determined with the heat of combustion of methane, $\Delta h_C = 50$ MJ/kg and the HRR curve, $\dot{Q}(t)$, (Fig. 1(b)), using $\dot{m}(t) = \dot{Q}(t)/\Delta h_C$.
- ***Thermo-physical properties:*** the temperature dependency of the specific heat capacity of the fluid mixture, c_p, is approximated by a polynomial function according to JANAF-tables of thermodynamics [32]. Thermo-physical parameters for the solid materials are assumed independent of temperature. Hence, the temperature dependent values of concrete presented in [33] are averaged and summarised in Table 2.

Table 2
Thermo-physical properties of the concrete tunnel lining.

Element	ρ (kg/m^3)	c_p (J/kg/K)	λ (W/m/K)
Tunnel lining	2400	1000	1

The main focus of the underlying CFD-analyses with the above described numerical set-up lies on the following issues and their dependency on the type of cross-section and the applied ventilation velocity:

- Temperature stratification in cross-sections at different longitudinal positions up- and downstream of the fire. Hereby, the identification of the 450 °C gas layer at ceiling level is of main interest. The fluid temperature of the 450 °C is suggested by the Swiss standard SIA 197/1 [15] and preliminary versions of the TSI SRT [16] to demonstrate the integrity of the tunnel structure for a period of 30 min [15] in order to allow appropriately-equipped firefighters to access the tunnel safely for the same duration of time.
- Temperature development at the surface and across the thickness of the concrete tunnel lining. These results are calculated by the fire code and are presented together with the evolution of the wall-heat fluxes. However, they only present a rough estimation of the solid temperatures as a higher spatial discretisation of the concrete lining as well as the consideration of temperature-dependent thermo-physical parameters of concrete are necessary in order to obtain more accurate results.

3.1. Results and discussion: Ventilation velocity 0.5 m/s

Vertical profiles of temperature at different longitudinal positions and time instants are depicted in Figs. 7 and 8 (see Appendix A.1, Fig. A.1 for further results). While the temperature profiles for the single-track tunnel are shown along the centre-line of the escape route ($z = 1.65$ m), they are plotted over the centre-line of the cross-section ($z = 0$ m) for the double-track tunnels. It can be observed that for all studied types of cross-sections a similar maximum fluid temperature which occurs in the vicinity of the fire source is predicted. Though the system cannot be considered in a stationary state as the tunnel lining is still heated and consumes thermal energy, changes in the fluid region decrease from 40 to 60 min and are considerably smaller compared to the period shortly after the growth phase. Compared to the double-track cross-sections, higher fluid temperatures are exhibited in the single-track cross-section at all positions $x \geqslant 0$ m (see Figs. 7 and 8, and Appendix A.1, Fig. A.1). This behaviour is explained with the

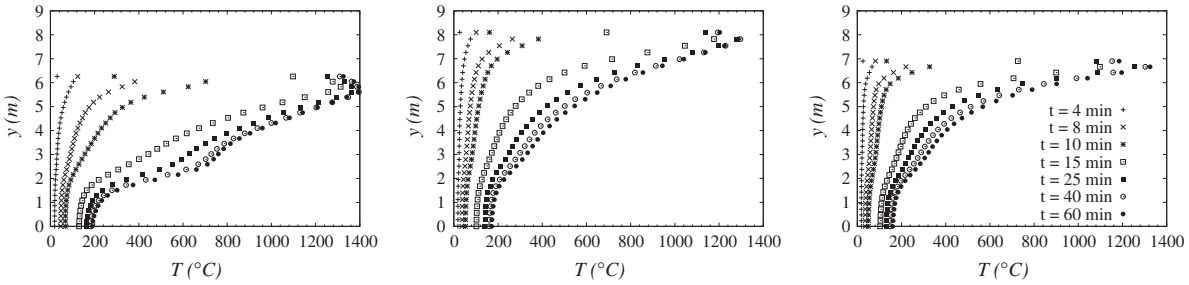

Fig. 7. Vertical temperature profiles at $x = 0$ m for the arched single-track (*left*, $z = 1.65$ m), arched double-track (*middle*, $z = 0$ m) and rectangular double-track (*right*, $z = 0$ m) cross-section for different time instants (0.5 m/s ventilation velocity).

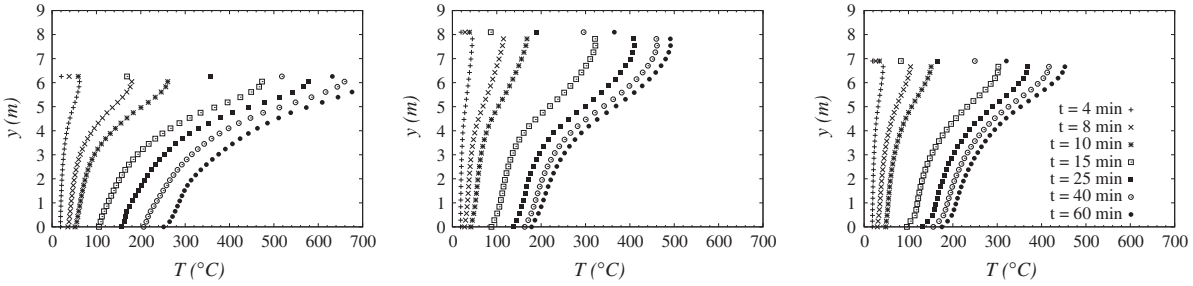

Fig. 8. Vertical temperature profiles at $x = 25$ m for the arched single-track (*left*, $z = 1.65$ m), arched double-track (*middle*, $z = 0$ m) and rectangular double-track (*right*, $z = 0$ m) cross-section for different time instants (0.5 m/s ventilation velocity).

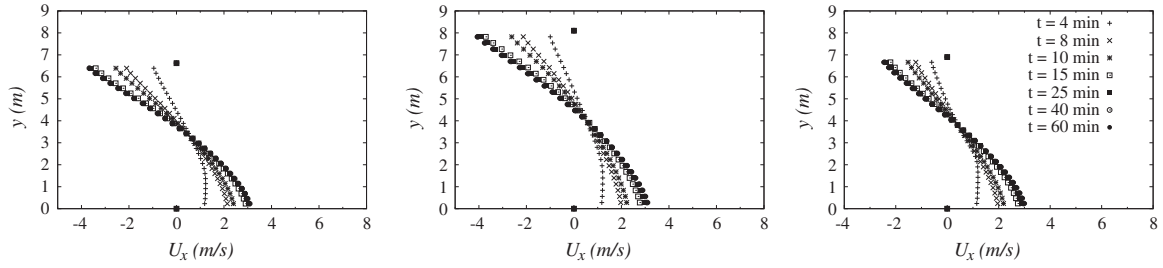

Fig. 9. Vertical profiles of horizontal velocity along the centre-line of the tunnel ($z = 0$ m) at $x = -20$ m for the arched single-track (*left*), arched double-track (*middle*) and rectangular double-track (*right*) cross-section for different time instants (0.5 m/s ventilation velocity).

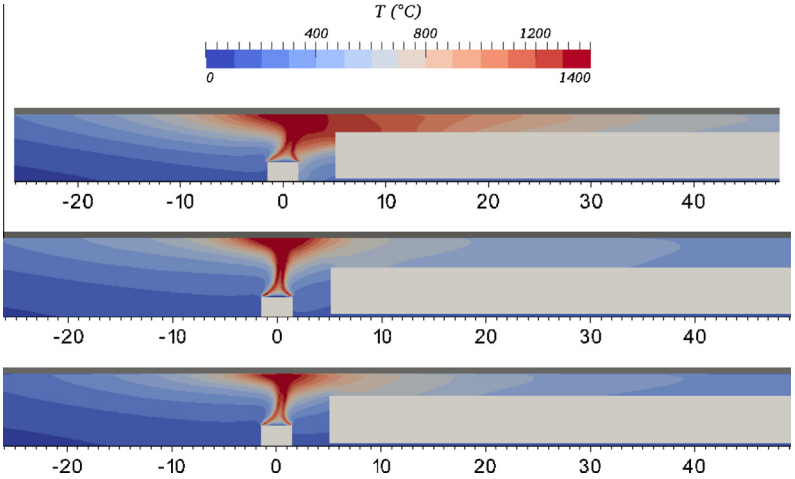

Fig. 10. Contour plots of temperature at $t = 60$ min for the arched single-track (*top*, $z = 0$ m), arched double-track (*middle*, $z = -2.3$ m) and rectangular double-track (*bottom*, $z = -2.3$ m) cross-section (dimensions in m, 0.5 m/s ventilation velocity).

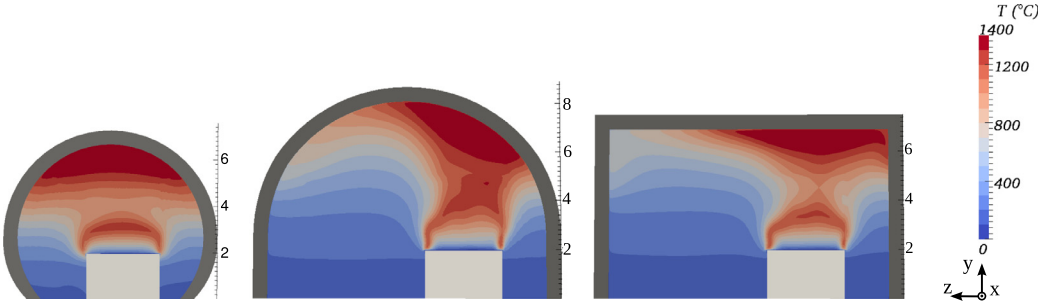

Fig. 11. Contour plots of temperature at $x = 0$ m for $t = 60$ min for the arched single-track (*left*), arched double-track (*middle*) and rectangular double-track (*right*) cross-section (dimensions in m, 0.5 m/s ventilation velocity).

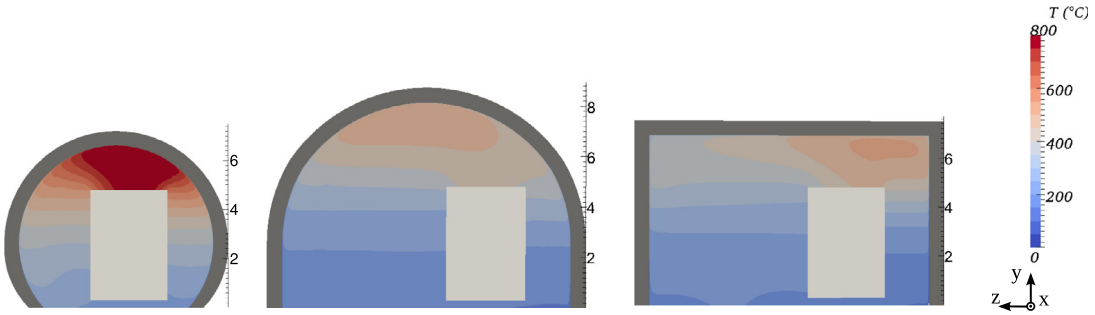

Fig. 12. Contour plots of temperature at $x = 25$ m for $t = 60$ min for the arched single-track (*left*), arched double-track (*middle*) and rectangular double-track (*right*) cross-section (dimensions in m, 0.5 m/s ventilation velocity).

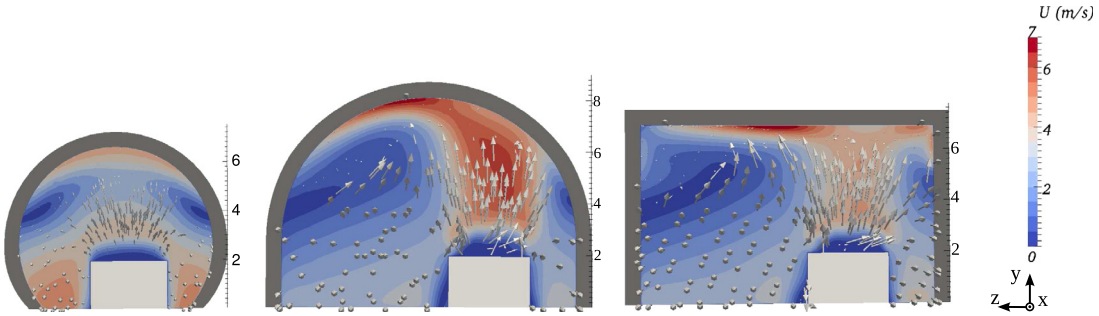

Fig. 13. Contour plots of velocity magnitude at $x = 0$ m for $t = 60$ min for the arched single-track (*left*), arched double-track (*middle*) and rectangular double-track (*right*) cross-section (dimensions in m, 0.5 m/s ventilation velocity).

Table 3
Longitudinal positions, x, of the 450 °C fluid temperature near the tunnel ceiling for the different cross-sections at specific time instants (0.5 m/s ventilation velocity).

t (min)	15	25	30	40	50	60
Single (arched): x (m)	32	46	50	58	64	69
Double (arched): x (m)	12	20	22	26	28	30
Double (rectangular): x (m)	13	20	22	26	28	31

smaller fluid volume in the single-track tunnel seen, e.g. in the ratio of the areas in the unblocked region between single- and double-track tunnel of $A_{ub,s}/A_{ub,d} = 0.46$ (see Table 1). Thus, with the same amount of released energy, the fluid is heated up stronger in case of the single-track tunnel which can be demonstrated with a simple energy balance. On the other hand, similar temperature levels are predicted for both double-track tunnels in consequence of the same cross-sectional area (see Figs. 8, 10, 11, 12 and Appendix A.1, Fig. A.2).

The vertical profiles of horizontal velocity at $x = -20$ m (see Fig. 9) show back-layering from the beginning of the fire. The back-flow of hot gases reaches the modelled tunnel inlet within the first 10 min of the fire for all cross-sections. This behaviour is expected as a result of the low ventilation velocity. While the simulation results show little influence of the cross-sectional type upstream of the fire, higher velocities are predicted for the single-track tunnel downstream of the fire (see Appendix A.1, Fig. A.3) as a result of a smaller ratio of the inflow area, A, and the unblocked area in the train section, A_{ub} (see Table 1). Moreover, in the vicinity of the fire at the upstream end of the train, the flame represents a blockage to the ventilation and leads to a further acceleration of the flow while it passes the fire. This effect is more pronounced in case of the single-track tunnel with a smaller cross-sectional area and a fire source of the same size as in the double-track tunnel. Hence, the flame exhibits a larger flame tilt angel in case of the single-track tunnel (see Fig. 10) as also observed during experiments presented in [34].

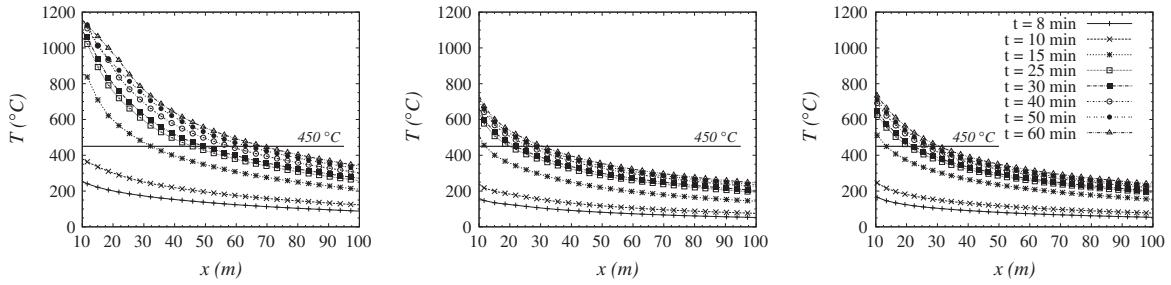

Fig. 14. Longitudinal temperature distribution near the tunnel ceiling for the arched single-track (y = 6.5 m and z = 0 m, *left*), arched double-track (y = 7.8 m and z = 0 m, *middle*) and rectangular double-track (y = 6.6 m and z = −2.3 m, *right*) cross-section for different time instants (0.5 m/s ventilation velocity).

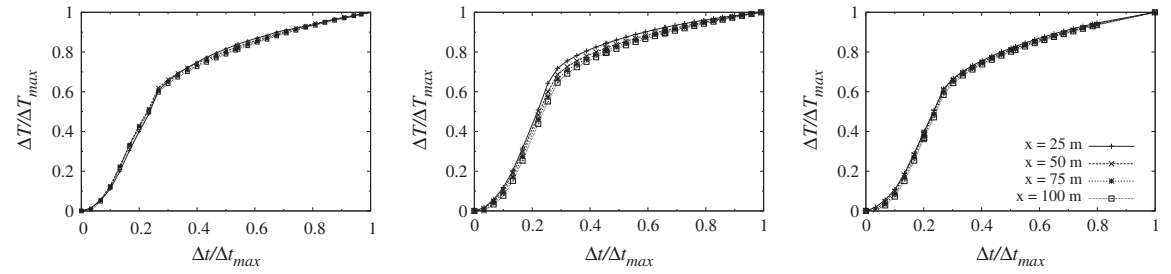

Fig. 15. Evolution of the fluid temperature near the tunnel ceiling in dimensionless form for the arched single-track (y = 6.5 m and z = 0 m, *left*), arched double-track (y = 7.8 m and z = 0 m, *middle*) and rectangular double-track (y = 6.6 m and z = −2.3 m, *right*) cross-section at different longitudinal positions, x (0.5 m/s ventilation velocity).

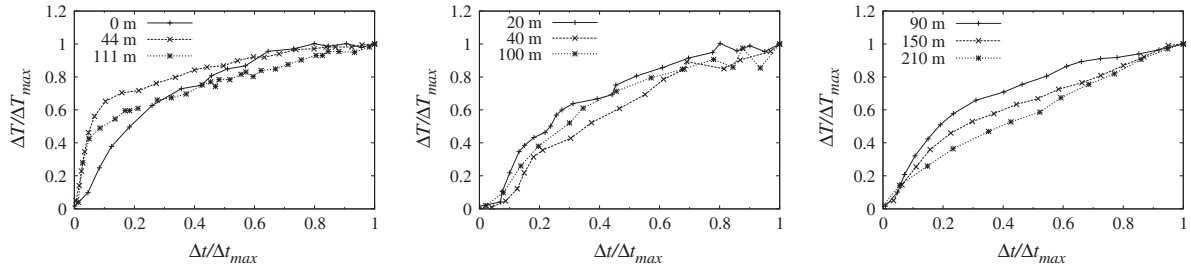

Fig. 16. Measured temperature evolution taken from three tunnel-fire experiments ([2] *left*, [5] *middle* and [36] *right*) in dimensionless form at different positions downstream of the fire.

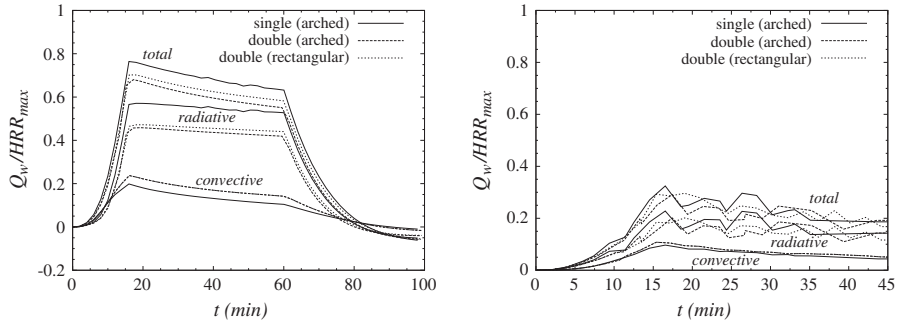

Fig. 17. Evolution of averaged absolute wall-heat fluxes at the concrete lining divided into convective and radiative part and normalised with the maximum HRR, HRR_{max}, for 0.5 (*left*) and 3 m/s (*right*) ventilation velocity.

For all investigated types of tunnel cross-section, the maximum fluid temperature is close to 1400 °C and is observed above the fire source after a fire duration of 60 min (see Figs. 10 and 11). A comparison with recent tunnel-fire experiments such as presented in [5,35], where depending on the type of fuel and the ventilation velocity maximum fluid temperatures between 600 °C and 1300 °C were measured, suggests a slight overestimation of the maximum temperature by the simulations. This was expected as the same behaviour was observed in the re-analysis of a tunnel-fire test presented in Section 2.1. In the present case, well-ventilated conditions cannot be expected above the fuel outlet ($y > 2$ m), where the back-flow of hot gases does not allow fresh air to reach the combustion region (see Appendix A.1, Fig. A.3). Thus, the estimation of the maximum fluid temperature must be considered as a

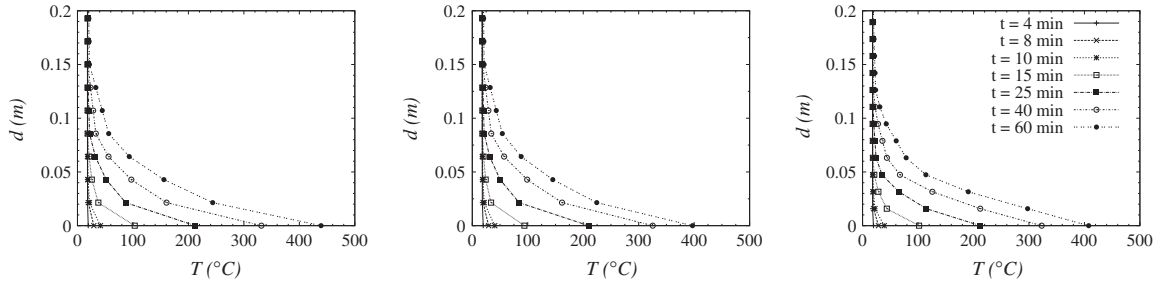

Fig. 18. Temperature profiles inside the tunnel lining at longitudinal positions where a fluid temperature of 450 °C occurs after 30 min (see Table 3) for the arched single-track ($x = 50$ m and $z = 0$ m, *left*), arched double-track ($x = 22$ m and $z = 0$ m, *middle*) and rectangular double-track ($x = 22$ m and $z = -2.3$ m, *right*) cross-section for different time instants (0.5 m/s ventilation velocity).

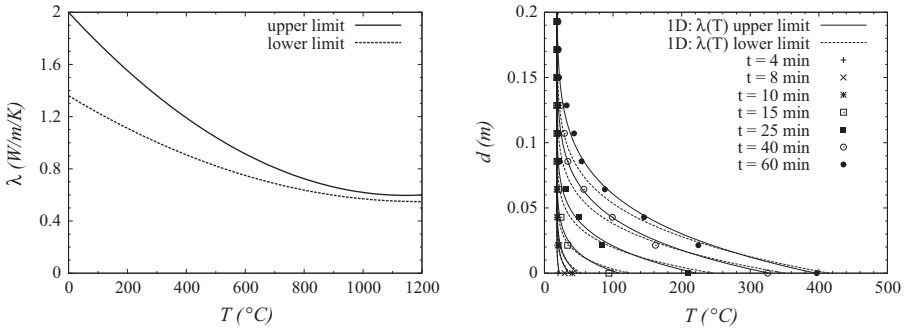

Fig. 19. Temperature dependency of thermal conductivity of concrete, λ, according to [33] (*left*) and comparison of temperature profiles inside the tunnel lining at $x = 22$ m for the arched double-track cross-section obtained with a 1D calculation (*lines*) and a 3D CFD simulation (*symbols*) (*right*, 0.5 m/s ventilation velocity).

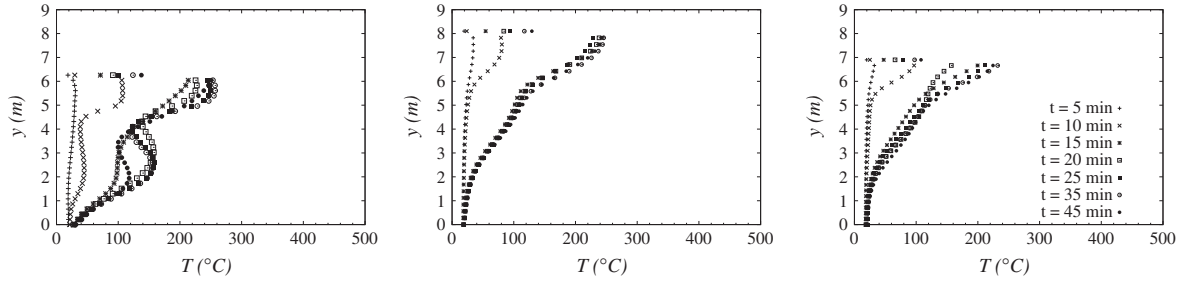

Fig. 20. Vertical temperature profiles at $x = 25$ m for the arched single-track (*left*, $z = 1.65$ m), arched double-track (*middle*, $z = 0$ m) and rectangular double-track (*right*, $z = 0$ m) cross-section for different time instants (3 m/s ventilation velocity).

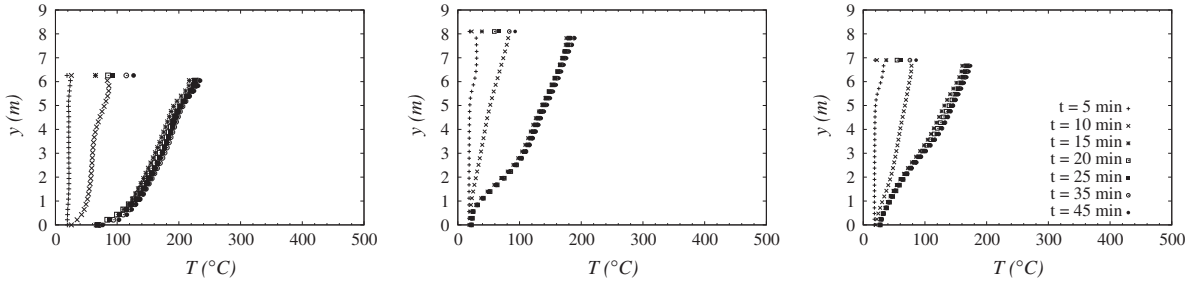

Fig. 21. Vertical temperature profiles at $x = 50$ m for the arched single-track (*left*, $z = 1.65$ m), arched double-track (*middle*, $z = 0$ m) and rectangular double-track (*right*, $z = 0$ m) cross-section for different time instants (3 m/s ventilation velocity).

worst-case scenario, whereas predictions at positions up- and downstream of the fire are more accurate (see Section 2.1).

While the typical vortices in the vicinity of the fire source are observed for both cross-sections (see Fig. 13), they are more pronounced in case of the arched cross-section due to the curved shape of the tunnel ceiling. Therefore, the hot gases concentrate in the highest region of the arch where the highest temperatures and velocities in the cross-sections at all longitudinal positions, x, are encountered (see, e.g. Fig. 12). In case of the rectangular cross-section, the hot gases – driven by buoyancy forces – hit the

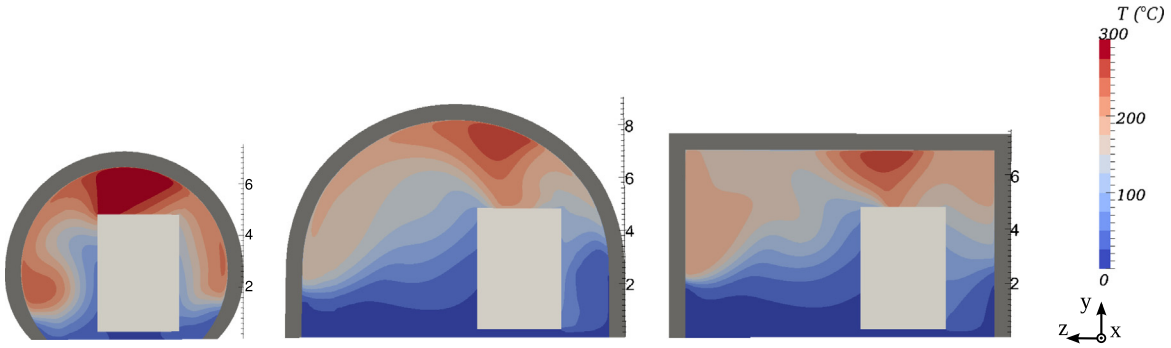

Fig. 22. Contour plots of temperature at $x = 25$ m for $t = 45$ min for the arched single-track (*left*), arched double-track (*middle*) and rectangular double-track (*right*) cross-section (dimensions in m, 3 m/s ventilation velocity).

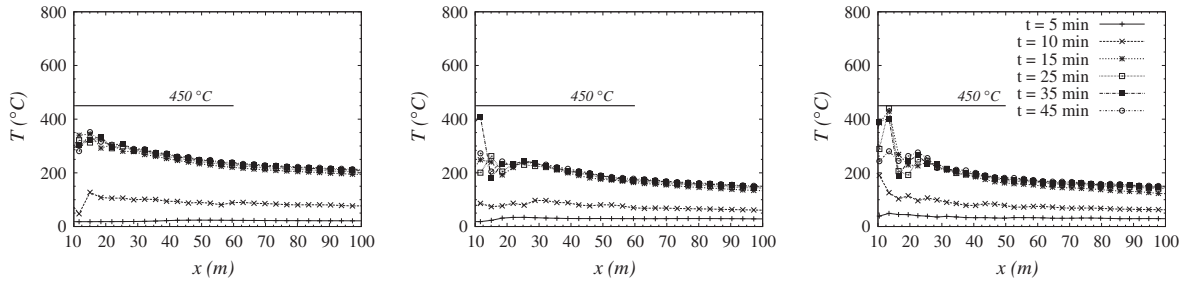

Fig. 23. Longitudinal temperature distribution near the tunnel ceiling for the arched single-track ($y = 6.2$ m and $z = 0$ m, *left*), arched double-track ($y = 7.8$ m and $z = 0$ m, *middle*) and rectangular double-track ($y = 6.7$ m and $z = -2.3$ m, *right*) cross-section for different time instants (3 m/s ventilation velocity).

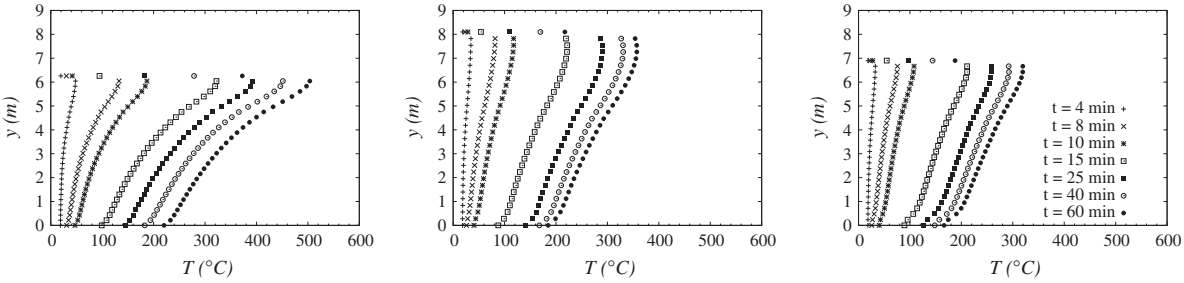

Fig. A.1. Vertical temperature profiles at $x = 50$ m for the arched single-track (*left*, $z = 1.65$ m), arched double-track (*middle*, $z = 0$ m) and rectangular double-track (*right*, $z = 0$ m) cross-section for different time instants.

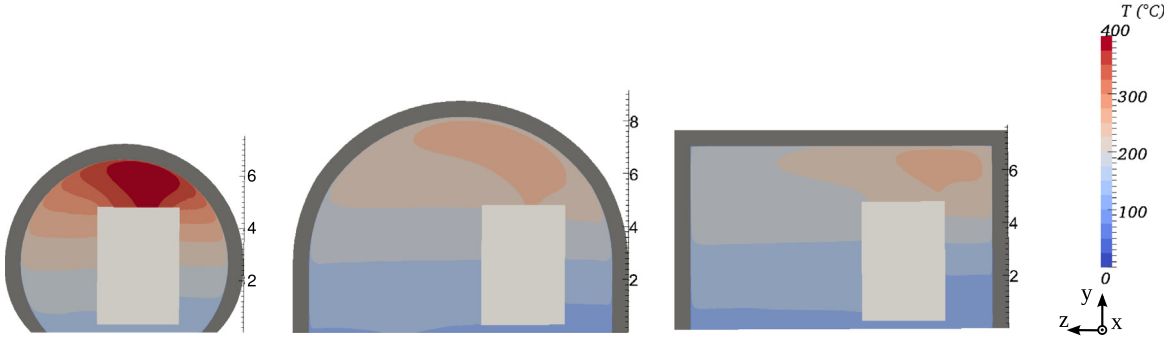

Fig. A.2. Contour plots of temperature at $x = 50$ m for $t = 60$ min for the arched single-track (*left*), arched double-track (*middle*) and rectangular double-track (*right*) cross-section (dimensions in m).

horizontal ceiling and travel directly up- and downstream of the fire. In consequence of this behaviour, the hot gases stay at the lateral position of the fire source in the cross-section for all values of x, whereas a trend towards a symmetric temperature distribution is seen for the arched cross-section further downstream of the fire (see Figs. 12 and Appendix A.1 Fig. A.2). Although similar velocity and temperature levels are predicted for both double-track tunnel cross-sections, this clearly shows the influence of the type of

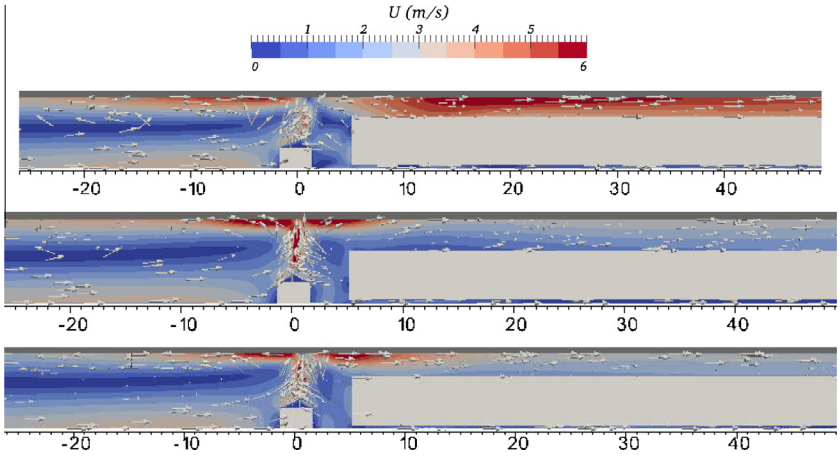

Fig. A.3. Contour plots of velocity magnitude at $t = 60$ min for the arched single-track (*top*, $z = 0$ m), arched double-track (*middle*, $z = -2.3$ m) and rectangular double-track (*bottom*, $z = -2.3$ m) cross-section (dimensions in m).

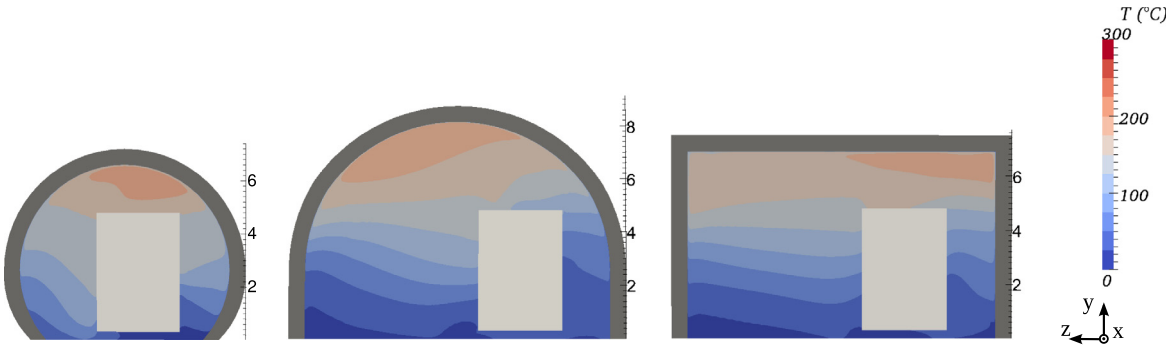

Fig. A.4. Contour plots of temperature at $x = 50$ m for $t = 45$ min for the arched single-track (*left*), arched double-track (*middle*) and rectangular double-track (*right*) cross-section (dimensions in m).

tunnel cross-section (arched or rectangular) on the temperature distribution in case of a tunnel fire. Together with the temperature stratification observed in all investigated shapes of cross-section (see, e.g. Figs. 7 and 8), which represent a non-constant temperature loading over the circumference for a fixed longitudinal position, the different temperature distributions within the cross-sections might have an implication for the structural stability of the tunnel lining.

The longitudinal temperature distributions near the tunnel ceiling for the three cross-sections are depicted in Fig. 14. The distributions are plotted along the centre of the arched tunnel cross-sections ($z = 0$ m) where the hot gases concentrate, whereas they are shown at the lateral position of the fire source ($z = -2.3$ m) for the rectangular cross-section. Fig. 14 shows the already mentioned higher fluid temperatures in case of a single-track tunnel. The longitudinal positions of the 450 °C fluid temperature near

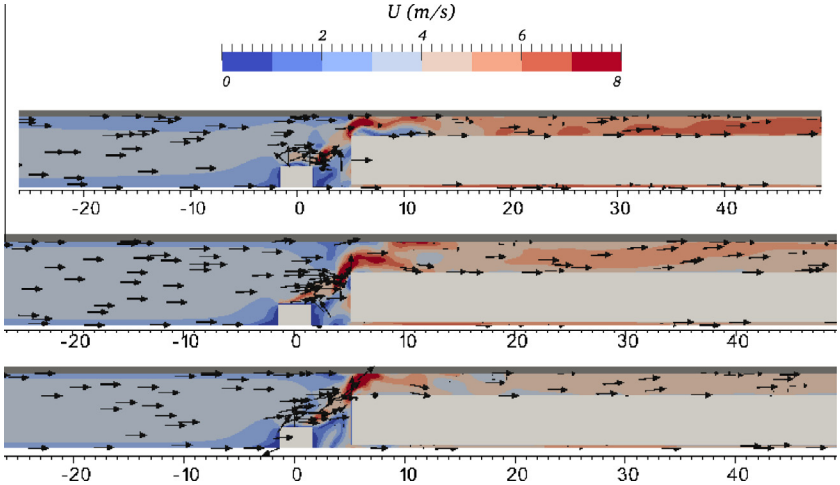

Fig. A.5. Contour plots of velocity magnitude at $t = 45$ min for the arched single-track (*top*, $z = 0$ m), arched double-track (*middle*, $z = -2.3$ m) and rectangular double-track (*bottom*, $z = -2.3$ m) cross-section (dimensions in m).

the tunnel ceiling, on which the assessment of the structural stability according to SIA 197/1 [15] and preliminary versions of the TSI SRT [16] must be based, are summarised in Table 3 for specific time instants. Table 3 shows that in the single-track tunnel the 450 °C gas layer moves approximately twice as fast as in case of a double-track tunnel in consequence of higher fluid temperatures and velocities (similar observations where made in [9]). Hence, firefighters have twice as much time for rescue operations in the double-track tunnel as in the single-track tunnel without risking the collapse of the concrete tunnel lining. The evolution of the fluid temperature near the tunnel ceiling at different downstream positions depicts an interesting result (see Fig. 15). The dimensionless representation, where the rise in temperature, $\Delta T = T - T_\infty$ (with T_∞ = 18 °C), is normalised with the maximum temperature rise at t_{max} = 60 min, i.e. $\Delta T_{max} = T_{max} - T_\infty$, is plotted against a dimensionless time, $\Delta t/\Delta t_{max} = (t - t_0)/(t_{max} - t_0)$ (with t_0 marking the start of the temperature rise), allows to obtain a single curve independent of the longitudinal position. Evaluating an energy balance at a specific longitudinal position shows, that the ratio of temperature rise, $\Delta T/\Delta T_{max}$, is proportional to the ratio of energies absorbed by a fluid element during the intervals Δt and Δt_{max}, respectively, which, as shown in Fig. 15, is constant for a specific time independent of the spatial position. Therefore, the rate of temperature rise at any longitudinal position is the same at a specific time.[1] To the best knowledge of the authors, no references concerning the dimensionless temperature-time curves could be found in the literature. However, an application of the same scaling on temperature measurements taken from different tunnel-fire experiments exhibit a trend towards a collapse of the dimensionless curves (see Fig. 16). Consequently, a single dimensionless temperature-time curve for any longitudinal position can be obtained and used together with the maximum fluid temperature at a specific location within the assessment of the structural safety of the tunnel.

Fig. 17 (*left*) shows the evolution of the averaged absolute wall-heat fluxes at the concrete tunnel lining normalised with the maximum HRR of 28 MW, where again very similar results are seen for the two double-track cross-sections. The total wall-heat flux is divided into a convective and a radiative part, exhibiting the dominance of radiative heat transfer to the tunnel lining for all studied cross-sections as already observed in experiments (see, e.g. [5]) or previous simulations of real-scale fire experiments (see, e.g. [17]). This confirms that radiative heat transfer needs to be taken into account in CFD-analyses of tunnel fires. In consequence of the increase in temperature of the tunnel lining during the fire, a decrease of both the convective and radiative wall-heat fluxes is observed for all three types of tunnel cross-sections from the moment the HRR reaches the constant value of 28 MW. The difference in the wall-heat fluxes for the different tunnel cross-sections is mainly seen in a higher radiative and, thus, in a higher total wall-heat flux in case of the arched single-track cross-section. This fact is explained with the higher fluid temperatures in the single-track tunnel compared to the double-track tunnels. Though the tunnel lining of the single-track cross-section absorbs more thermal energy, the remaining energy released by the fire leads to a higher temperature rise than in case of the double-track tunnels as a result of an approximately 1.8 times greater inflowing mass flux of fresh air in the latter cases (see Table 1).

Fig. 18 depicts temperature profiles inside the concrete tunnel lining at different time instants in the middle of the ceiling (z = 0 m) for the arched cross-sections and in the lateral position of the fire source (z = −2.3 m) for the rectangular cross-sections at longitudinal positions where a fluid temperature of 450 °C occurs after 30 min (see Table 3). For all studied tunnel cross-sections it can be seen that at the surface of the tunnel lining (d = 0 m) a temperature greater than 400 °C is only attained between 40 min $\leqslant t \leqslant$ 60 min though the fluid temperature at these positions reached 450 °C already at t = 30 min. This rather large difference between fluid and solid temperature can be attributed to the fact that a coarse grid was applied in the solid region and that the temperature dependency of the thermo-physical parameters of concrete was not taken into account. The latter becomes evident when comparing the temperature dependency of the concrete's thermal conductivity, λ, i.e., lower and upper limit, adopted from [33] (see Fig. 19 (*left*)) with the constant value of 1 W/m/K used within the analyses. During most of the time the thermal conductivity and, thus, the penetration of the thermal front is underestimated, also leading to a slightly higher propagation speed of the 450 °C isotherm within the fluid than in the case where a temperature dependent λ according to Fig. 18 is considered. Hence, a comparison of a 1D calculation of temperature distributions inside the concrete lining and the profiles obtained by the CFD simulations for the arched double-track cross-section at x = 22 is shown in Fig. 19 (*right*). In the 1D calculation, the heat-conduction equation was solved by considering convective and radiative heat transfer towards the surface exposed to the fire in terms of a net specific wall-heat flux, $q_{w,tot} = \alpha_c(T_f - T_w) + \epsilon\sigma_{SB}(T_f^4 - T_w^4)$ [31] on a fine grid of 100 cells. The evolution of the fluid temperature, T_f, was taken from the respective CFD simulation and the temperature dependency of the concrete's thermal conductivity from Fig. 19 (*left*). The convective heat-transfer coefficient, α_c, and the surface emissivity of concrete, ϵ, were set to 25 W/m^2/K [31] and 0.7 [33], respectively. Great deviations of surface temperatures between the 1D calculation (*lines*) and the CFD simulation (*symbols*) are observed at the beginning of the fire in the order of 20 °C for a temperature of 200 °C (10%), whereas a decrease in the difference is seen with increasing surface temperatures (see Fig. 19 (*right*)). Though it is not possible to model radiative heat transfer to surrounding colder walls with the 1D calculation, the results suggest a two step approach in order to obtain the most accurate temperature profiles inside the concrete lining: In the first step, fluid temperatures are determined in a 3D CFD simulation, in the second step, the 1D heat-conduction equation is solved by using the fluid temperatures from the previous CFD simulation, taking into account the temperature dependency of the thermo-physical parameters of concrete ($\rho(T)$, $c_p(T)$ and $\lambda(T)$) and, in case the risk of spalling is of interest, thermo-hydro-chemical transport processes (as demonstrated, e.g. in [8]). It is however worth mentioning, that the proposed approach does not consider the absorption of heat by the tunnel lining due to phase change of liquid water present in the concrete, which in turn influences the temperature evolution of the fluid. A remedy represents the thermal coupling of the fluid flow with the thermo-hydro transport processes in the concrete as suggested in [37].

3.2. Results and discussion: Ventilation velocity 3 m/s

The simulation results show fluctuations of the flow field around the upstream end of the train for all studied types of cross-sections. These fluctuations are induced by separation of the bulk flow when hitting the sharp edges of the modelled train at the upstream end and result in strong variations of the flow parameters (see, e.g. Fig. 20). The cause of the fluctuations seen in the numerical simulations, where the applied numerical set-up (turbulence model, wall functions, grid, etc.) is not meant to resolve flow separation at sharp edges, needs further investigation as to the authors' knowledge such a behaviour was not observed in similar tunnel-fire experiments. However, the effect of the flow separation strongly reduces for downstream positions of

[1] In [5], a similar shape of the temperature evolution at different positions during tunnel-fire tests were noticed.

$x \geqslant 25$ m (see Figs. 20 and 21), where the comparison of the modelled turbulent viscosity and the molecular viscosity indicates a smaller dominance of turbulence than in the region around the upstream end of the train. Thus, the results can still be used to illustrate a trend for the case of a tunnel fire where the ventilation of 0.5 m/s is increased to 3 m/s.

As expected, no back-layering occurs (see Appendix A.2, Fig. A.5). The vertical profiles of temperatures at $x = 25$ m along the centre-line of the escape route ($z = 1.65$ m) for the single-track cross-section and over the centre-line of the cross-section ($z = 0$ m) for the double-track tunnels at different time instants exhibit the mentioned fluctuations (see Fig. 20). At the positions further downstream, the flow becomes more stable and no significant temperature changes are observed between $t = 35$ and 45 min (see Fig. 21). Moreover, the temperature levels are strongly reduced compared to the case of 0.5 m/s ventilation velocity which is also seen in the contour plots of temperature (see Fig. 22, and Appendix A.2, Fig. A.4). Therefore, in none of the depicted cross-sections hot gases exceeding a temperature of 450 °C are observed as depicted in the longitudinal temperature distributions at ceiling level (see Fig. 23). This is explained with the fact, that the six times higher ventilation velocity introduces a greater mass flux of fresh air, diluting and cooling the hot combustion gases. In addition, the higher ventilation speed leads to a faster transport of the hot gases out of the tunnel.

Unlike in case of a ventilation velocity of 0.5 m/s where big differences in fluid temperatures were observed between the single- and double-track tunnels, this behaviour cannot be seen for a ventilation velocity of 3 m/s (see, e.g. Figs. 20 and 22). Slightly higher fluid temperatures are predicted for the single-track tunnel but in fact very similar temperature levels are observed for the investigated cross-sections. On the other hand, considering the distribution of temperature within the cross-section, the same trend as for a ventilation velocity of 0.5 m/s is exhibited, i.e. hot gases concentrating in the arch of the ached cross-sections, whereas hot gases move along the lateral position of the fire source for the rectangular cross-section (see Fig. 22 and Appendix A.2, Fig. A.4).

The fluctuations of the flow field are also seen in the evolution of the averaged absolute wall-heat fluxes (see Fig. 17 (*right*)) for all types of cross-sections. As already observed in the previous simulations with 0.5 m/s ventilation velocity, a trend of decreasing heat fluxes with increasing duration of the fire is exhibited. The faster transport of hot gases out of the tunnel also reduces the heat transfer to the tunnel lining and, hence, the total wall-heat flux. Compared with the wall-heat fluxes in the case of a ventilation velocity of 0.5 m/s, the higher ventilation velocity reduces the absorbed thermal energy by approximately 50% (see Fig. 17). However, it has to be mentioned that the current approach of prescribing the same HRR-time curve for tunnel fires with different ventilation velocities does not allow to reproduce the influence of forced ventilation on the development of the fire's HRR as observed in tunnel-fire experiments (see, e.g. [6,38]).

4. Conclusions

The results of CFD simulations modelling a 28 MW fire inside railway tunnels of different cross-sections, i.e. an arched single-track, an arched double-track and a rectangular double-track cross-section, were presented. The consequences of the tunnel fire were investigated under ventilation conditions of 0.5 and 3 m/s. The predictions of temperature distributions within the cross-sections as well as longitudinal temperature distributions at ceiling level shall provide the basis for the assessment of the tunnel's structural stability in case of a fire. Hereby, the focus lay on cross-sectional temperature distributions as well as on the identification of the longitudinal position of the 450 °C gas layer at ceiling level. 450 °C represents the fluid temperature on which the assessment of the structural stability according to the Swiss Standard [15] and the preliminary version of the TSI SRT [16] must be based.

As expected, higher levels of temperature and velocity magnitudes were observed in the single-track than in the double-track tunnel for each of the ventilation velocities which is in consequence of the smaller fluid volume. For the double-track tunnels, similar levels of temperature and velocity were predicted as a result of the same cross-sectional area. The influence of the type of cross-section was mainly seen in the distribution of flow parameters over the cross-section. Hot gases propagated up- and downstream of the fire at the lateral position of the fire source (i.e. above the blockage) for the rectangular tunnel, whereas they concentrated in the arch of the arched tunnels. The observed temperature stratification and different temperature distributions within all studied cross-sections might have an implication on the structural performance of the respective tunnel.

For a ventilation velocity of 0.5 m/s, the 450 °C gas layer at ceiling level propagated to approximately 30 m downstream of the fire after 60 min for the double-track cross-sections, whereas a distance of $x = 69$ m was observed for the single-track cross-section, thus, the hot gas layer moved more than twice as fast in the latter case. On the other hand, fluid temperatures dropped dramatically for a ventilation velocity of 3 m/s, as the six times higher ventilation velocity transported the hot combustion gases out of the tunnel faster. Consequently, fluid temperatures were lower than 450 °C in all cross-sections and the higher ventilation velocity allowed to reduce the wall-heat fluxes by approximately 50%. Furthermore, unlike in case of 0.5 m/s ventilation velocity, similar temperature levels were predicted in both the single- and double-track tunnels with a ventilation velocity of 3 m/s.

An investigation of the temperature profiles inside the concrete tunnel lining lead to the conclusion, that a two-step approach for the calculation of the most accurate temperature profiles inside the concrete lining should be followed: the fluid temperatures which were determined in a 3D CFD simulation in the first step, serve as input for the solution of the 1D heat-conduction in the second step, taking into account the temperature dependency of the thermo-physical parameters of concrete and, in case it is of interest, the risk of spalling.

Acknowledgments

The authors thank the members of the *"OpenFOAM Stammtisch"* at Vienna University of Technology for fruitful discussions as well as Mr. Heissenberger (ÖBB-Infrastruktur AG, Engineering Services, Tunnelbau) and Mr. Bopp, who supported this work with valuable comments.

The computational results presented in this paper have been achieved in part using the Vienna Scientific Cluster (VSC).

This research was financially supported by the Austrian Ministry for Transport, Innovation and Technology (bm.vit) via the KIRAS-project (Austrian security research program) 824781 "Sicherheit von Hohlraumbauten unter Feuerlast – Entwicklung eines Struktursimulationstools (Safety of underground structures under fire loading – Development of a structural simulation tool)". This support is gratefully acknowledged!

Appendix A

A.1. Ventilation velocity 0.5 m/s

See Figs. A.1–A.3.

A.2. Ventilation velocity 3 m/s

See Fig. A.4 and A.5.

References

[1] Haack A. Technical report Part 1 – design fire scenarios. Tech rep. Thematic Network FIT – Fire in Tunnels; 2007.
[2] Bettis RS, Jagger SF, Wu Y. Interim validation of tunnel fire consequence models: summary of phase 2 tests. Internal report. Health and Safety Executive Research and Laboratory Services Division. IR/L/FR/93/11; 1993.
[3] Ingason H. Heat release rate measurements in tunnel fires. SP report 1994:08. Swedish National Testing and Research Institute; 1994.
[4] Ingason H, Lönnermark A. Heat release rates from heavy goods vehicle trailer fires in tunnels. Fire Safety J 2005;40:646–68.
[5] Lönnermark A, Ingason H. Gas temperatures in heavy goods vehicle fires in tunnels. Fire Safety J 2005;40:506–27.
[6] Lönnermark A. On the characteristics of fires in tunnels. PhD thesis. Department of Fire Safety Engineering, Lund Institute of Technology, Lund University; 2005.
[7] Ring T. Experimental characterization and modeling of concrete at high temperatures – structural safety assessment of different tunnel cross-sections subjected to fire loading. PhD thesis. Institute for Mechanics of Materials and Structures, Vienna University of Technology; 2012. ISBN: 978-3-9502481-6-6.
[8] Zeiml M, Lackner R, Pesavento F, Schrefler BA. Thermo-hydro-chemical couplings considered in safety assessment of shallow tunnels subjected to fire load. Fire Safety J 2008;43(2):83–95.
[9] Tuovinen H, Holmstedt G, Bengtson S. Sensitivity calculations of tunnel fires using CFD. Fire Technol 1996;32(2):99–119.
[10] Wu Y, Bakar M. Control of smoke flow in tunnel fires using longitudinal ventilation systems – a study of the critical velocity. Fire Safety J 2000;35:363–90.
[11] Lee S, Ryou H. A numerical study on smoke movement in longitudinal ventilation tunnel fires for different aspect ratio. Build Environ 2006;41:719–25.
[12] Vauquelin O, Wu Y. Influence of tunnel width on longitudinal smoke control. Fire Safety J 2006;41:420–6.
[13] Wang H. Numerical and theoretical evaluations of the propagation of smoke and fire in a full-scale tunnel. Fire Safety J 2012;49:10–21.
[14] Blanchard E et al. Experimental and numerical study of fire in a midscale test tunnel. Fire Safety J 2012;47:18–31.
[15] Zürich S. Schweizer norm 505 197/1: Projektierung Tunnel – Bahntunnel. Schweizerische Normen-Vereinigung SNV, SIA 197/1:2003 ed.; 2004.
[16] Agency ER. Technical specification for interoperability on safety in railway tunnels (TSI SRT). 06 2012. Preliminary draft version 2.0, retrieved August; 2012. <http://www.era.europa.eu/Document-Register/Pages/era-con-2012-05-int.aspx>.
[17] Amouzandeh A. Development and application of a computational fluid dynamics code to predict the thermal impact on underground structures in case of fire. PhD thesis. Institute for Mechanics of Materials and Structures, Vienna University of Technology; 2012. ISBN: 978-3-9502481-5-9.
[18] OpenCFD. OpenFOAM 1.7.1 – the open source CFD toolbox – user guide. OpenCFD Limited; 2010. <http://www.openfoam.com>.
[19] Novozhilov V. Computational fluid dynamics modeling of compartment fires. Progr Energy Combust Sci 2001;27:611–66.
[20] van Maele K, Merci B. Application of two buoyancy-modified k–ε turbulence models to different types of buoyant plumes. Fire Safety J 2006;41:122–38.
[21] Raithby G. Discussion of the finite-volume method for radiation, and its application using 3-D unstructured mesh. Numer Heat Transf 1999;35(4):389–405.
[22] Modest M. Radiative heat transfer. 2nd ed. Academic Press; 2003.
[23] Yeoh GH, Yuen KK. Computational fluid dynamics in fire engineering. Elsevier; 2008 [chapter 3]. ISBN: 978-0-7506-8589-4.
[24] Magnussen B. The eddy dissipation concept – a bridge between science and technology. In: Proceedings of the ECCOMAS thematic conference on computational combustion, Lisbon, Portugal; 21–24 June, 2005.
[25] Union International des Chemins de Fer (UIC). "Rules governing application of the enlarged GA, GB, GB1, GB2, GC and GI3 gauges," codex 506 VE. Union International des Chemins de Fer; 2008. ISBN 2-7461-1374-0.
[26] AG DB. Ergebnisbericht zur Beurteilung von Bränden an Schienenfahrzeugen als Bemessungsbrände zur brandschutztechnischen Auslegung von oberirdischen Personenverkehrsanlagen der Deutschen Bahn AG. Tech rep. DB Station & Service, Fachstelle Brandschutz, Frankfurt am Main; September 2000.
[27] Ingason H. Design fire curves for tunnels. Fire Safety J 2009;44:259–65.
[28] Langner V, Bopp R. Semmering-Basistunnel Neu – Technischer Bericht Lüftungskonzept. Tech rep. Gruner GmbH Ingenieure und Planer. Plannummer: 5510-EB-0600AL-00-0001-F02; 2010.
[29] Baum H, McCratten K, Rehm R. Three dimensional simulation of fire plume dynamics. In: Hasemi Y, editor. Fire safety science, proceedings of the fifth international symposium. The International Association for Fire Safety Science; 1997. ISBN: 4-9900625-5-5.
[30] Casey M, Wintergerste T. European research community on flow, turbulence and combustion: best practice guidlines. Version 1.0; January 2000.
[31] European Committee for Standardization. Eurocode 1: actions on structures – Part 1–2: general actions – actions on structures exposed to fire. EN 1991-1-2:2002 ed.; 2002.
[32] McBride B, Gordon S, Reno M. Coefficients for calculating thermodynamic and transport properties of individual species. NASA Technical Memorandum 4513, National Aeronautics and Space Administration; 1993.
[33] European Committee for Standardization. Eurocode 2: design of concrete structures – Part 1–2: general rules – structural fire design. EN 1992-1-2:2004 ed.; 2004.
[34] Oka Y, Atkinson G. Control of smoke flow in tunnel fire. Fire Safety J 1995;25:305–22.
[35] Haack A, Meyeroltmanns W, Cabos H. Verhalten von Schienenfahrzeugen in Stahl- bzw. Aluminiumbauweise bei Tunnelbränden. Forschungsbericht P 570. Studiengesellschaft Stahlanwendung e.V., Düsseldorf; 2001.
[36] Hu L et al. Experimental studies on fire-induced buoyant smoke temperature distribution along tunnel ceiling. Build Environ 2007;42:3905–15.
[37] Schrefler B, Codina R, Pesavento F, Principe J. Thermal coupling of fluid flow and structural response of a tunnel induced by fire. Int J Numer Methods Eng 2011;87:361–85.
[38] Carvel R, Beard A, Jowitt P, Drysdale D. The influence of tunnel geometry and ventilation on the heat release rate of a fire. Fire Technol 2004;40:5–26.